observation after 1min of light illumination, while the lowermost curve is the observation of the clusters after its leaving for one night with the previous light illumination of the clusters by 38.5 min. As it is seen from the comparison of lowermost and its previous curves, the difference is negligible. It says that suspension of clusters is rather stable with a time, however its external perturbation by light source results in the changes of peak intensities and small blue-shift.

In order to investigate the $(CdSe)_n$ clusters having time dependence, we have repeated calculations with the same cutoff energies for three different supercell sizes: $a = 16$Å, 20Å and 24Å.

3. FIRST PRINCIPLE CALCULATION

We first performed structural optimization by means of the ultrasoft-pseudopotential program (VASP) [4] to obtain the locally stable wurtzite structure as well as the most stable endohedral cage structure that has already been done in Refs. [1-3]. The geometries of the resulting optimized $(CdSe)_{13}$ clusters are shown in Figs. 2(a) and (b), respectively, for the endohedral cage and wurtzite structures, while the corresponding bulk geometries before relaxation are shown in Figs. 2(a') and (b'). The result for the endohedral cage structure is the same as that given in Refs. [1-3].

Note that there is no corresponding bulk geometry for the endohedral cage structure in Fig. 2(a).

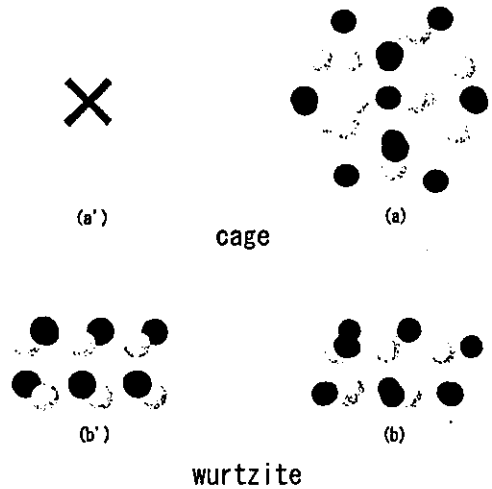

Fig. 2 Optimized $(CdSe)_{13}$ geometries for the (a) endohedral cage and (b) wurtzite structures. Left figures, (a'), (b'), show the corresponding bulk geometries before relaxation (a cross in (a') means that the endohedral cage structure has no bulk counterpart). White and black spheres are Cd and Se atoms, respectively.

Next we performed the calculation of the dielectric function for the two clusters shown in Figs. 2(a) and (b). For this purpose, we used the all-electron mixed basis approach [5-7], in which each LDA wave function is expanded in the linear combination of both atomic orbitals (AO's) and plane waves (PW's). We used an fcc lattice with the unit cell size corresponding to the nearest neighbor distance between clusters being equal to a. All core and valence AO's are generated by Herman-Skillman's atomic code [8] within the non-overlapping atomic spheres, and the 4 Ry is assumed for the PW's. The dielectric function is evaluated within the random phase approximation (RPA) via the equation [9]

$$\varepsilon(q,\omega) = 1 - \frac{8\pi}{\Omega q^2}\sum_{k}\sum_{\lambda}\sum_{\nu}\frac{\left|\langle k+q,\lambda|e^{iq\cdot r}|k,\nu\rangle\right|^2\left[f_0(\varepsilon_{k+q,\lambda}) - f_0(\varepsilon_{k,\nu})\right]}{\varepsilon_{k+q,\lambda} - \varepsilon_{k,\nu} - \omega - i\delta}, \quad (1)$$

where the summations with respect to the level indices λ and ν run over all levels (here we chose 1,000 levels), k is the wave vector inside the first Brillouin zone and denotes f_0 the Fermi-Dirac distribution function; the prefactor 2 means the spin multiplicity and Ω is the volume of the unit cell.

4. RESULT

Figs. 3(a) and (b) show our results of the dielectric function for the endohedral cage structure and wurtzite structure, respectively.

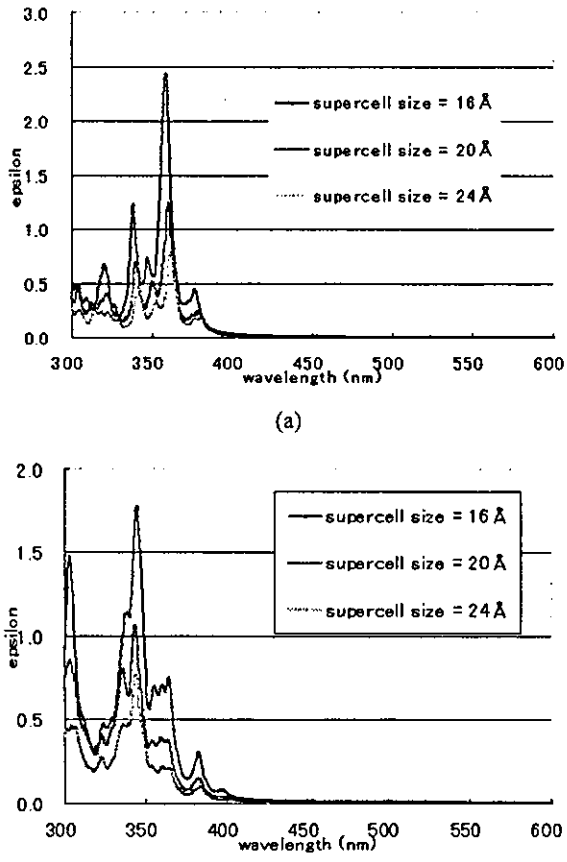

Fig. 3 Imaginary part of dielectric function of $(CdSe)_{13}$ clusters for (a) the endohedral cage and (b) the wurtzite structures. In the figures, three curves (from top to bottom) represent the results for different supercell sizes, 16Å, 20Å and 24Å, respectively.

If we compare three curves in Figs. 3 (a) and (b), we find that the effect of the supercell size is not negligible, because the peaks of supercell size = 16Å are much higher than those of supercell size = 24Å. The larger the intercluster distance, the lower the height of the peaks. This is mainly because of the factor $1/\Omega$ in Eq.(1).

The peak positions are, however, not sensitive to the supercell size. In Fig. 3(a) for the endohedral cage structure, there are two peaks around 340nm and 360nm. On the other hand, the results for the wurtzite structure in Fig. 3(b) have the following characteristics:

(1) Two peaks around 300-310nm and 340nm.
(2) Shoulder around 350-360nm.
(3) Long tail in lower energy side.

The shoulder of (2) may correspond to the right side of the experimental peaks around 350nm of lower curves in Fig. 1.

5. INTERPRETATION OF EXPERIMENT

Based on the fair agreements between theoretical calculation and experimental results, the observed spectra are interpreted as follows:

From the above result, under light illumination the certain number of clusters having cage like structure decomposes by a well-known effect of size selective photoetching. This seems to have a linear character with respect to the time of light illumination. The more the time of illumination, the more clusters decompose and a part of the rest of clusters changes the geometry from cage structure to wurtzite structure. It effects as well as to the local arrangement of the organic molecules surrounding $(CdSe)_{13}$ which changes due to the electric fields caused by the charged rest of $(CdSe)_{13}$ clusters. Then, we would imagine that the rest of clusters, solvent and surfactants molecules gradually rearrange their positions and structure to stabilize whole system.

The decrease of number of clusters leads to the increase of effective distance between $(CdSe)_{13}$ clusters. Then, we could argue that the upper curves observed for low illumination times correspond to the samples that have a short intercluster distance and are characteristic of the endohedral cage structure, while the lower curves observed for long times illuminations correspond to the samples which have a large intercluster distance and are characteristic of wurtzite structure.

6. SUMMARY

In summary, we have optimized two (endohedral cage and wurtzite) structures of $(CdSe)_{13}$ and calculated their dielectric response function in the RPA on the basis of the LDA in density functional theory. We have compared its imaginary part with the optical absorption spectra measured experimentally for the $(CdSe)_{13}$ sample dissolved in toluene. We conclude that most of the created clusters in solution have the endohedral cage structure. The experimental results show some aging effect of sample as noted in the optical spectrum. It may be caused by a change in the geometry of the clusters from the endohedral cage structure to the wurtzite structure. For this explanation, our theoretical results are consistent with the experimental observations. More experimental investigation, however, is necessary for sample preparation to discuss further. The calculations for the larger size cluster, of $(CdSe)_{33}$ and $(CdSe)_{34}$ is now on progress and will be reported in near future.

7. ACKNOWLEDGEMENT

The authors are grateful for continuous support of the HITAC SR8000 supercomputing facilities that are owned by the Computer Science Group at the Institute for Materials Research, Tohoku University. VK thankfully acknowledges the hospitality at the IMR and the support form JSPS.

REFERENCES

[1] Y. Barnakov, R. Sivamohan, I. Dimitruk, T. Kudo, T. Nirasawa, T. Arai, K. Tohji, O. Terasaki, A. Kasuya, V. Kumar and Y. Kawazoe, Proc. Int. Symp. On Cluster Assembled Mater. (IPAP Conf. Series 3) pp. 56-58 (2002).

[2] A. Kasuya, R. Sivamohan, Y. Barnakov, I. Dmitruk, T. Nirasawa, S. Mamykin, V. Romanyuk, K. Tohji, V. Jeyadevan, K. Shinoda, T. Kudo, O. Terasaki,, Z. Liu, V. Kumar, R. Belosludov, V. Sundararajan, and Y. Kawazoe, to be published.

[3] V. Kumar, R. Belosludov, V. Sundararajan, Y. Kawazoe, and A. Kasuya, to be published.

[4] G. Kresse and J. Furthmüller, Comput. Mater. Sci. **6**, 15 (1996); Phys. Rev. B **54**, 11 169 (1996).

[5] K. Ohno, Y. Maruyama, K. Esfarjani, Y. Kawazoe, N. Sato, R. Hatakeyama, T. Hirata and M. Niwano, Phys. Rev. Lett. **76**, 3590 (1996).

[6] K. Ohno, F. Mauri and S. G. Louie, Phys. Rev. B **56**, 1009 ((1997).

[7] S. Ishii, K. Ohno and Y. Kawazoe, Mater. Trans. JIM **40**, 1209 (1999).

[8] F. Herman and S. Skillman, "Atomic Structure Calculations" (Prentice-Hall, New Jersey, 1963).

[9] S. L. Adler, Phys. Rev. **126**, 413 (1962).

(Received October 13, 2003; Accepted April 24, 2004)

Transactions of the Materials Research Society of Japan 29 [8] 3727-3729 (2004)

Dynamics on Electronic Excitation in Chemical Reaction

Takahiro Sawada[1], Jian Wu[2], Yoshiyuki Kawazoe[3] and Kaoru Ohno[1]
[1]Department of Physics Graduate School of Engineering, Yokohama, National University,
79-5 Tokiwadai, Hodogaya-ku, Yokohama 240-8501, Japan
Fax: 81-45-338-3020, e-mail: d03gd221@ynu.ac.jp, ohno@ynu.ac.jp
[2]Center for Advanced Study, Tsinghua University, Beijing 100084, P. R. China
Fax: 86-10-6278.1886, e-mail: wu@catu.tsinghua.edu.cn
[3]Institute for Materials Research, Tohoku University, Sendai 980-8577
Fax: 81-22-215-2052, e-mail: kawazoe@imr.edu

Carrying out simplified theoretical simulations using the time-dependent Schrödinger equation on the basis of the time-dependent density functional theory (for electrons) coupled with the Newtonian equation of motion (for nuclei), we find that a chemical reaction, $Li_2+H_2 \rightarrow 2LiH$, takes place by the double excitation from the highest occupied molecular orbital (HOMO) level to the lowest unoccupied molecular orbital (LUMO) level. Along the reaction path, a level crossing occurs automatically between the highest occupied and lowest unoccupied levels and the electronic excited state changes smoothly into the electronic ground state leaving a kinetic energy of the molecules, i.e., a rapid energy transfer from the electronic excitation to the molecular motion of the order of 10 femto seconds.
Key words: time-dependent Schrödinger equation, spectral method, and a level crossing

1. INTRODUCTION

The electronic excitation opens new reaction channels of chemical reactions. It is interesting to study the chemical reactions at electronic excited states. When we simulate the dynamics on electronic excited states, we can avoid to use the potential energy surface (PES) [1,2] which is the most popular approach nowadays. Instead we can integrate directly the time-dependent *Schrödinger* equation (TDSE) within the framework of the time-dependent density functional (TDDF) theory [3,4]. The merit of doing it is to treat the wavepacket states as well as the steady states. In this paper we focus on the chemical reaction induced by double excitation in a simple system composed of Li_2 and H_2 and carry out the TDSE first-principle molecular dynamics (FPMD) simulation. In what follows, we present an explicit result of the dynamical simulation of $Li_2+H_2 \rightarrow 2LiH$.

2. THEORY

In integrating the TDSE

$$i\frac{\partial}{\partial t}\Psi_j(t)=H(t)\Psi_j(t), \qquad (1)$$

with respect to time, we introduce the spectral method [5]. This spectral method uses the eigenstate $\varphi_k(t)$ and the eigenvalue ε_j of the Hamiltonian $H(t)$, which satisfies

$$H(t)\varphi_k=\varepsilon_k\varphi_k. \qquad (2)$$

Here, $H(t)$ denotes just the electronic part. Since it depends on time, this eigenvalue problem must be solved at each time. Therefore, φ_k and ε_k have also the time dependence, although it is not expressed explicitly. The oscillation of the Hamiltonian $H(t)$ may appear for time which is typically 100-1000 times smaller than the time step for the atomic motion and continue for a time interval of the order of a femtosecond. However, when the electronic states are not far from steady states, the Hamiltonian would not significantly change in time inside this transient time interval. We expand the wavepackets $\Psi_j(t)$ in terms of the eigenstates $\varphi_k(t)$ at the same time,

$$\Psi_j(t)=\sum_k c_{jk}(t)\varphi_k, \qquad (3)$$

where

$$c_{jk}(t)=\langle\varphi_k \mid \Psi_j(t)\rangle. \qquad (4)$$

Hence, the basic time step Δt can be set as large as the time scale in which the Hamiltonian changes, one may integrate the TDSE as follows:

$$\Psi_j(t+\Delta t)=\sum_k c_{jk}(t)\exp(-i\varepsilon_k\Delta t)\varphi_k. \qquad (5)$$

In real numerical treatments, the sum with respect to the eigenstates in Eq. (5) is evaluated only over a finite number of low-lying exited states as well as the ground state. Those low-lying existed states should include also the free-electron continuum states above the vacuum levels. So we use the all-electron mixed basis approach [6-8] which uses plane waves (PW's) together with atomic orbitals (AO's) as basis functions. The all-electron mixed basis approach enables us to represent correctly the free-electron continuum states as well as the bound and resonance states within the all-electron formalism. For the treatment of exchange-correlation terms, we use the local-density approximation (LDA). For the Newtonian equation of motion for nuclei, we use the forces calculated as a derivative of the total energy, as formulated by Ho et al. [9]

3. RESULT AND DISCUSSION

We first consider the case of the electronic ground state. Assuming zero initial velocity, we start the

TDSE-FPMD simulation. The initial atomic geometry of Li_2 and H_2 molecules are placed to face each other with a distance on the order of the bond length with which the molecules appears in the reaction. Figure 1 shows the time-evolution of atomic motion. The two molecules, Li_2 and H_2, repel each other with slight interamolecular vibrations forming two isolated molecules. The trajectory is essentially the same as that obtained by the usual Car-Parrinello-type molecular dynamics simulation [4]. The time-evolution of the energy expectation values is shown in Fig. 2.

Next we consider the case of the doubly excited state from the highest occupied molecular orbital (HOMO) level to the lowest unoccupied molecular orbital (LUMO) level at the same initial geometry. The resulting trajectory [Fig. 3] is obviously quite different from the previous Fig. 1. This reaction yields two isolated LiH molecules. The motion of the atoms may be characterized as vibrations along the Li-H bond and repulsion between the LiH molecules. The initial H-H and Li-Li bond are broken very quickly. The balance of the Li-H bond is achieved near its ground-state bond length. The time-evolution of the energy expectation values is shown in Fig. 4 for doubly excited state.

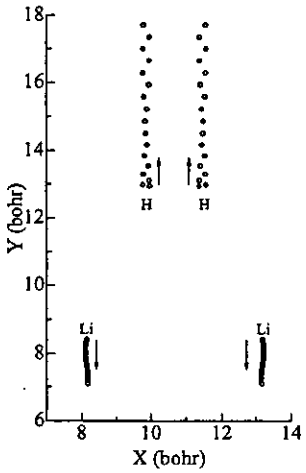

Fig. 1 The time evolution of atomic motion in the simulation starting from the ground state. The abscissa and ordinate represent, respectively, in the X and Y directions

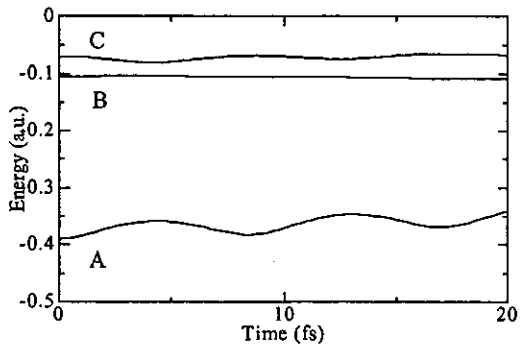

Fig. 2 The time-evolution of the energy expectation values of the valence electrons starting from the ground state. Level B is the highest occupied molecular orbital level. Level C is the lowest unoccupied molecular orbital level.

As seen in Fig. 4, a level crossing occurs between the highest occupied (C) and lowest unoccupied (B) levels approximately 10fs after the initial excitation. Since the present reaction proceeds nearly on the stationary state of the Hamiltonian at each time, it is possible to give a clear physical picture of the present reaction. We may consider only 1*s* orbital of H and 2*s* orbital of Li. Then, there are four possible electron levels, A, B, C and D, regardless of the spin multiplicity. First, level A has the lowest energy, representing the fully bonding molecular orbital (MO). Next, intermediate level B represents the bonding Li-Li and H-H and the anti-bonding Li-H MO, while level C represents the anti-bonding Li-Li and H-H and the bonding Li-H MO. Lastly, level D, having the highest energy, is characterized by the fully anti-bonding MO, although it is not shown in Figs. 2 and 4 because it exceeds the upper limit of vertical scale. Obviously there exists a bonding tendency between the Li and H atoms in levels A and C, and an anti-bonding tendency between the Li and H atoms in level B and D. Therefore, in the simulation starting from the ground state, in which level B is occupied and level C is empty, the two Li atoms attract each other and so do the two H atoms, because of the bonding tendency in the occupied levels A and B. On the other hand, in the simulation starting from the doubly excited state, in which level B is empty and level C is occupied, the Li and H atoms attract each other because of the bonding tendency in the occupied levels A and C. In fact, as shown in Fig. 4, levels A and C become closer to be degenerated and anti-bonding empty level B becomes higher when the Li and H atoms make bonds.

As a result of these bonding and anti-bonding tendencies, the level crossing occurs automatically when new molecules are synthesized. The occupied level C, which was originally higher than the empty level B, goes down due to the formation of the Li-H bonds and becomes lower than the empty level B without interlevel hopping. And the electronic energy plus potential energy between nuclei is lowered during this reaction, and the excess energy is all transferred into the kinetic energy of the atoms. In the way, the level crossing plays a key role in the process of the relaxation from the double excitation.

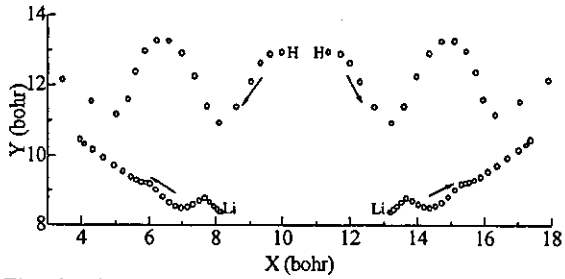

Fig. 3 The time evolution of atomic motion in the simulation starting from the doubly excited state

4. CONCLUSION

In this paper, by integrating the coupled equations of the TDSE-FPMD numerically with respect to time, we found a chemical reactions, $Li_2+H_2 \rightarrow 2LiH$, in the double excitation. Along the reaction, a level crossing occurs between the HOMO and LUMO levels, according to Fukui's frontier orbital theory and Woodward-Hoffmann law [10-12]. From the present simulation, we can propose

a mechanism for relaxation of the reaction by the double excitation: electronic excited state changes smoothly into the electronic ground state leaving a kinetic energy of the atoms.

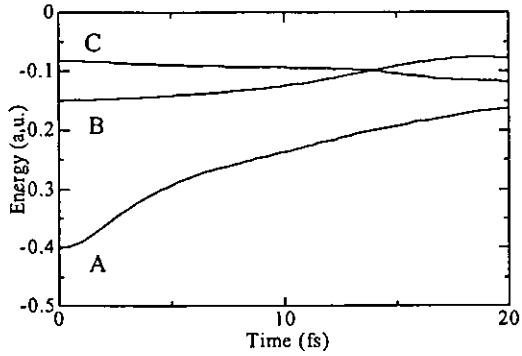

Fig. 4 The time-evolution of the energy expectation values of the valence electrons starting from the doubly excited state. By the double excitation, the electrons move from the highest occupied orbital level to the lowest unoccupied molecular orbital level. Level B is empty and levels A and C are occupied.

5. ACKNOWLEDGEMENT

The authors are grateful for the support of the HITAC SR8000 supercomputing facilities that are owned by the Computer Science Group at the Institute for Materials Research, Tohoku University.

REFERENCES

[1] S. S. C. Ammal and P. Venuvanalingam, *J. Phys. Chem. A* **104**, 10859 (2000).

[2] E. Bodo, Gianturco, R. Martinazzo and M. Raimondi, *Eur. Phys. J. D* **15**, 321 (2001).

[3] E. Runge and E. K. U. Gross, *Phys. Rev. Lett.* **52**, 997 (1984).

[4] see for a review, K. Ohno, K. Esfarjani and Y. Kawazoe, "Computational Materials Science", Solid-State Sciences, Vol. **129** (Springer-Verlag, Berlin, Heidelberg, 1999). : From Ab Initio to Monte Carlo Methods

[5] J. J. Sakurai, "Modern Quantum Mechanics" (The Benjamin/Cummings Publishing Company 1985) Sect. **2.1**

[6] K. Ohno, F. Mauri, and S. G. Louie, *Phys. Rev. B* **87**, 1009 (1997).

[7] T. Ohtsuki, K. Ohno, K. Shiga, Y. Kawazoe, Y. Maruyama and K. Masumoto, *Phys. Rev. Lett.* **81**, 967

[8] S. Ishii, K.Ohno, Y.Kawazoe, and S. G. Louie, *Phys. Rev. B* **63**, 155104 (2001).

[9] K. M. Ho, C. Elsässer, C. T. Chan and M. Fähnle, *J. Phys.*: Condens. Matter 4, 5189 (1992).

[10] K. Fukui, T. Yonezawa and H.Shingu, *J. Chem. Phys.* **20**, 722 (1952).

[11] R. B. Woodward and R. Hoffmann, *J. Am. Chem. Soc.* **87**, 395 (1965).

[12] J. Simons, "Quantum Mechanics in Chemistry" (Oxford Univ. Press, 1997)

(Received October 13, 2003; Accepted April 24, 2004)

Reprinted from

PHYSICAL REVIEW
B

CONDENSED MATTER AND MATERIALS PHYSICS

NOVEMBER 2004
15(I)

Water adsorption on Ti-doped silicon clusters

Hiroaki Kawamura,[1,2] Vijay Kumar,[1,3] and Yoshiyuki Kawazoe[1]
[1]*Institute for Materials Research (IMR), Tohoku University, 2-1-1 Katahira Aoba-ku, Sendai 980-8577, Japan*
[2]*New Frontiers Research Laboratories, Toray Industries, Inc., 1111 Tebiro, Kamakura, Kanagawa 248-8555, Japan*
[3]*Dr. Vijay Kumar Foundation, 45 Bazaar Street, Chennai 600 078, India*

Published by
THE AMERICAN PHYSICAL SOCIETY

Volume 70 **Third Series** **Number 19**

Water adsorption on Ti-doped silicon clusters

Hiroaki Kawamura,[1,2] Vijay Kumar,[1,3] and Yoshiyuki Kawazoe[1]
[1]*Institute for Materials Research (IMR), Tohoku University, 2-1-1 Katahira Aoba-ku, Sendai 980-8577, Japan*
[2]*New Frontiers Research Laboratories, Toray Industries, Inc., 1111 Tebiro, Kamakura, Kanagawa 248-8555, Japan*
[3]*Dr. Vijay Kumar Foundation, 45 Bazaar Street, Chennai 600 078, India*
(Received 10 February 2004; published 4 November 2004)

Ab initio calculations have been performed on adsorption of H_2O molecules on Ti-doped silicon clusters $TiSi_n$ using the ultrasoft pseudopotential method within the generalized gradient approximation. Our results show that for $n=13$ and larger clusters adsorption of H_2O on $TiSi_n$ could be difficult due to low binding energies. All these clusters have cage structures with the metal atom surrounded by the silicon atoms. On the other hand, smaller clusters with $n<13$ have the metal atom partially covered by Si atoms in a basket structure so that it is available for reaction with a water molecule. This leads to significantly higher binding energies of a water molecule on such clusters. These results are in excellent agreement with the available experimental data, which show significant decrease of H_2O adsorption on clusters with $n>12$.

DOI: 10.1103/PhysRevB.70.193402 PACS number(s): 73.22.−f, 71.15.Nc, 61.46.+w

Currently, metal (M) encapsulated silicon clusters are attracting much attention[1–14] because of their interesting properties and structures. These could serve as building blocks for nanomaterials and miniature devices. Cage structures, especially fullerene, cubic, and Frank-Kasper type have been predicted for MSi_n ($n=14-16$) by Kumar and Kawazoe[1] with their unique characteristics. Subsequently, many theoretical studies have been made to determine the properties of clusters with M=Cr,[2–4] Fe,[1,5,6] and other M atoms.[7–10] In addition, large abundances have been obtained for 15 and 16 Si atom clusters with one M atom[11,14] and low reactivity of MSi_{12}, M=Cr, Mo, W has been obtained with hydrogen.[3,12] Recently, adsorption behavior and electron affinities of Ti-doped clusters have been studied which are important for the understanding of their stability as well as for their usage. Kumar *et al.*[13] have studied the ionization potentials and electron affinities of $M@Si_{16}$, M=Ti and Zr clusters. Ohara *et al.*[14] have reported the experimental results of not only the mass spectra but also the adsorption of H_2O molecules on Si_nTi clusters. These studies could also serve as important benchmarks to understand the structures of MSi_n clusters.

The results of these experiments show that adsorption of H_2O on $Ti@Si_n$ clusters could be found only up to $n=12$. For larger clusters, the reaction ratio decreases significantly and from $n=15$ onwards it becomes almost zero. Considering the well known high reactivity of H_2O with Ti, the vanishingly small adsorption of H_2O molecules on $TiSi_n$ clusters with $n>12$ is thought to be due to the encapsulation of Ti by Si atoms so that Ti atom is not accessible to H_2O molecules for reaction. However, this idea could not explain all the experimental results *a priori*. For example, a hexagonal prism structure can exist for $n=12$ similar to the one[3,12] for WSi_{12}. As the hexagonal faces are not capped, it is possible that H_2O could interact with Ti by intruding into the relatively open hexagonal rings. If it can, the experiments are not the proof for the formation of cage structures. Moreover, at the outset it is not clear if the Si atoms should be weakly interacting with H_2O if a cage is formed. The atomic structures of smaller clusters with M=Ti have not yet been understood. In order to understand the interaction of H_2O with $TiSi_n$ clusters, the determination of the structures of $TiSi_n$ clusters in the wide range of sizes under the same calculation conditions is indispensable. So far theoretical studies are mostly on a few selected sizes. Therefore, we have first performed calculations for determining the lowest energy structures of $Ti@Si_n$ clusters with $n=8-16$. Based on these results, further calculations have been done on adsorption of a H_2O molecule on $TiSi_n$ clusters.

The calculations are performed using the *ab initio* ultrasoft pseudopotential method,[15,16] within the spin-polarized generalized gradient approximation of Perdew and Wang[17] for the exchange-correlation energy. A simple cubic supercell with size 15 Å for $n=8-14$ and 18 Å for other larger clusters is used with periodic boundary conditions. The Brillouin zone is represented by the Γ point. For Si and O we consider only the outer valence electrons, but for Ti we also included $3p$ atomic core states as valence states. The structural optimizations have been performed using the conjugate gradient method such that the residual force on each ion was less than 0.001 eV/Å. The total energy has been calculated up to an accuracy of 0.0001 eV. In order to determine the lowest energy structures we used several candidates as initial guesses. Although one cannot still be completely sure of the minimum energy structures, we believe that our results should represent lowest energy structures. This belief is further supported by the good agreement with experiments of the adsorption behavior of a water molecule. Here we report the structures of $TiSi_n$ briefly from the point of view of the adsorption of H_2O. A detailed discussion of the low lying structures and the growth behavior has been given in Ref. 18. While under the experimental conditions of finite temperatures, there could be more than one isomer present for some clusters if the energy difference is small and vibrational contribution to entropy as well as zero point energy may affect the ordering of free energies, we have considered primarily the lowest energy structures. We believe that our studies demonstrate sufficiently clearly the main findings of the experiments.

Figure 1 shows the lowest energy structures of $TiSi_n$ [(a)–(i)] and two interesting isomers [(j) and (k)] for $TiSi_{12}$ and $TiSi_{13}$, respectively. These can be classified into basket and

 ©2004 The American Physical Society

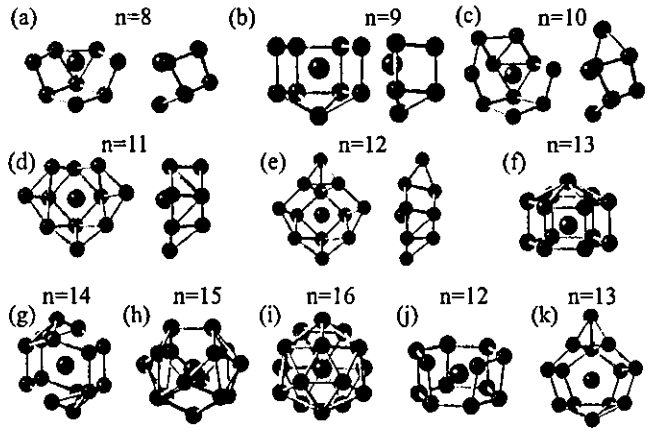

FIG. 1. (Color) (a)–(i) The lowest energy structures of $TiSi_n$ ($n=8-16$) with (j) and (k) as the local minimum structures for $TiSi_{12}$ and $TiSi_{13}$, respectively. Ti atom is shown by a bigger ball (green).

cage structures. As seen in Fig. 1, the most favorable structures for $n=8-12$ are basket type. In these clusters the Ti atom is partially covered with Si and therefore it could interact with H_2O. Furthermore, we find that a hexagonal prism structure is not the lowest energy structure for $TiSi_{12}$. It prefers a basket-type structure and it is the largest cluster for $Ti@Si_n$ with the basket structure. Figure 1(j) shows a hexagonal prism-like cage structure for $n=12$, but one Si-Si bond is quite elongated (not bonded in Fig. 1), with the bond length of 3.00 Å. This can exist as a local minimum with 0.273 eV higher energy as compared to the basket isomer. The larger atomic radius of Ti as compared to Cr or W could be a reason for the opening of this hexagonal prism structure besides the fact that the number of electrons in the case of Ti is different, and this could also lead to a different structure to be of the lowest energy. We also calculated a hexagonal antiprism structure and it lies 0.680 eV higher in energy. Therefore, it is also a local minimum isomer. From these results we conclude that cage structures are not suitable for $n=12$. Cage structures are, however, formed for $n>12$ (Fig. 1). We calculated a basket isomer for $n=13$ [Fig. 1(k)] and it lies 0.878 eV higher in energy than the cage isomer. An interesting point is that $n=13$ and 14 have open (not capped) hexagonal rings so that H_2O molecule might intrude into the clusters to interact with Ti. Thus, the possibility of adsorption of H_2O molecules could not be determined only by these structures.

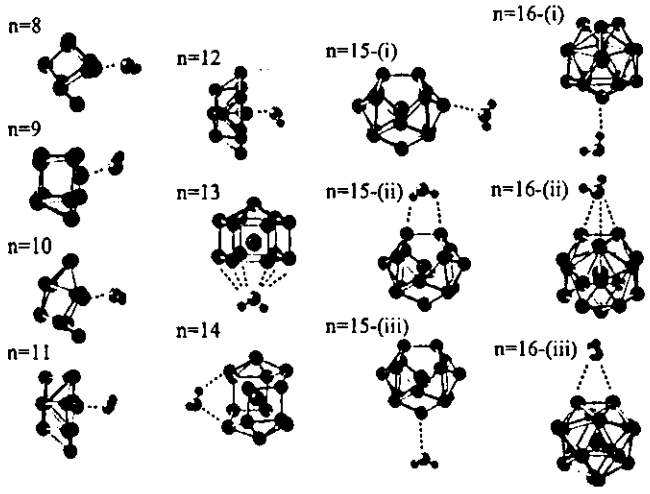

FIG. 2. (Color) Optimized arrangements of H_2O interacting with $TiSi_n$ clusters. For $n=15$ and 16, three different approaches of water molecule to the cluster are shown. The nearest bonds between the H_2O and the cluster are shown by dashed lines. The small (big) balls represent H (O) atoms in the H_2O molecule.

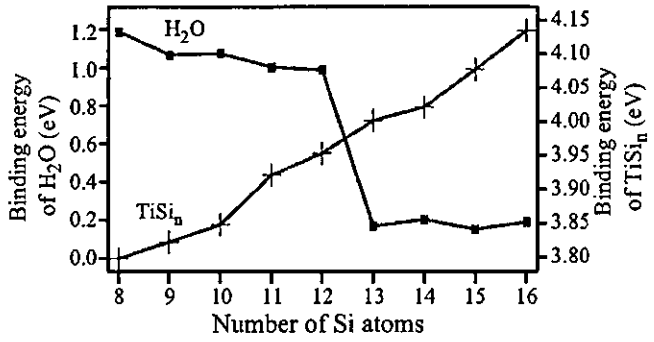

FIG. 3. Interaction energies (left scale) between $TiSi_n$ and H_2O ($n=8-16$). The atomic arrangements for $n=15$ and 16 are shown, respectively, as 15-(i) and 16-(i) in Fig. 2 which have the largest interaction energy in each size. The right scale shows the binding energy per atom of $TiSi_n$ clusters.

As in experiments of H_2O adsorption all clusters are positively charged, we also determined[18] the structures of cation clusters following the results of the neutral clusters. It is found that the structural differences between the neutral and cation clusters are not significant. For $n=12$ the energy difference[18] between the cage and the basket isomers is not large (0.273 eV) and we also studied cations of both these isomers. Our calculated energy difference between the cations is 0.387 eV and the basket isomer remains more stable than the cage isomer. More details of these studies will be published separately.[18] The calculations of adsorption of H_2O on $TiSi_n$ have been performed by initially putting an H_2O molecule with O facing the Ti atom of the lowest energy isomer of $TiSi_n$ for $n=8-12$ (basket structures) and in front of the center of the open hexagonal ring for $n=13$ and 14 cage isomers. For $n=15$ and 16 cage isomers there are no such open sites for the H_2O molecule to adsorb. Therefore,

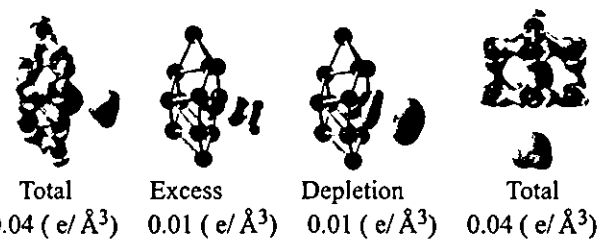

FIG. 4. (Color) Electronic-charge density isosurfaces for $TiSi_n$ ($n=12$ and 13) interacting with H_2O. Excess and depletion charges for $TiSi_{12}$ are calculated from the difference between the charge of $TiSi_n$ interacting with H_2O and the sum of the charges of the isolated $TiSi_n$ and H_2O.

TABLE I. Binding energy (BE) per atom for $TiSi_n$ clusters, optimized distances between Ti and O (d_{Ti-O}), and interaction energies (E) between $TiSi_n$ and H_2O. The three values for $n=15$ and 16 correspond to three configurations of H_2O. In the case of $n=13$, oxygen is nearly equidistant from Si and Ti atoms, but for $n=14-16$, the Ti-O bond is quite long and the interaction is actually with silicon atoms.

n	BE/atom (eV)	Optimized d_{Ti-O} (Å)	E (eV)
8	3.798	2.14	1.188
9	3.822	2.16	1.069
10	3.848	2.16	1.076
11	3.921	2.20	1.004
12	3.953	2.19	0.989
13	4.001	3.78	0.169
14	4.021	4.52	0.204
15-(i)	4.077	5.64	0.152
15-(ii)	4.077	5.80	0.137
15-(iii)	4.077	6.03	0.078
16-(i)	4.135	6.26	0.189
16-(ii)	4.135	5.71	0.156
16-(iii)	4.135	5.87	0.156

three directions of approach have been selected for the H_2O molecule. The optimized arrangements and the distances between Ti and O are shown in Fig. 2 and in Table I, respectively.

In the basket isomers an H_2O molecule stays near the cluster and the distance between Ti and O after the optimization lies in the range of 2.14 to 2.20 Å. In the most important sizes of $n=13$ and 14, very weak or no adsorption could be found in experiments. It is found that in these cases the H_2O molecule moves away from the cluster and the final converged Ti-O bond lengths in $n=13$ and 14 are large (3.78 and 4.52 Å, respectively) and the interaction is more with the Si atoms. For $n=13$, the Si-O bond lengths are in the range of 3.65–3.71 Å, which are nearly equal to the Ti-O bond. However, the change in the position of Ti atom after adsorption of H_2O is quite small. Therefore, we conclude that interaction of H_2O is predominantly with Si atoms. In the case of $n=14$, the bare $Ti@Si_{14}$ cage structure is quite distorted and O interacts with one Si atom such that the Si-O bond length is shorter (2.93 Å). In addition, one H interacts with a Si atom and the Si-H bond length is 2.61 Å. Accordingly in this case the interaction of H_2O is slightly stronger. This leads to a slight enhancement in the interaction energy. For $Ti@Si_{15}$ and $Ti@Si_{16}$ only weak interaction with Si atoms has been found for all three approaching directions, as expected. However, after optimization the directions of H_2O to the clusters are not the same. As seen in Fig. 2, for $Ti@Si_{15}$ we considered two top sites and one bridge site as initial configurations with, O facing the cluster. In the two cases of top sites O interacts with the cage atoms [15-(i) and 15-(iii)], while in the case of the bridge site [15-(ii)], the two H atoms interact with the Si bridge atoms. The Si-H bond lengths are 2.92 and 3.15 Å. The O-Si bond lengths are 2.83 and 3.35 Å for isomers 15-(i) and 15-(iii), respectively. For $Ti@Si_{16}$, O points to the cluster side when it is on a bridge site (Si-O bond lengths 3.50 Å) joining two Si hexagons [Fig. 2 (16-iii)] or on a triangle (Si-O bond lengths 3.48–3.58 Å) joining three Si hexagons [Fig. 2 (16-ii)]. However, when H_2O is placed on top of a capping atom (of Si hexagons), then H points towards the cluster, as shown in Fig. 2 (16-i) with Si-H bond length of 2.70 Å. The Si-H as well as Si-O bond lengths in these clusters are much longer as compared to the covalent bond length of about 1.5 Å for Si-H and 1.65 Å for Si-O. This different result indicates weak interaction between H_2O and the clusters.

In order to further quantify the interaction, we estimate the interaction energy from $E(TiSi_n)+E(H_2O)-E(TiSi_n+H_2O)$. It is given in Table I and Fig. 3. The interaction energy in the basket isomers ($n=8-12$) is about 1 eV and except for $n=8$, it lies in a quite small range, the decrease being only 0.080 eV in going from $n=9$ to $n=12$. Therefore, adsorption of H_2O is energetically favorable for $n=8-12$, with a small decrease in the interaction energy as the size increases. On the other hand, the stability of clusters becomes better with an increase in size, as can be seen in Fig. 3. After $n=16$, there is a decrease in the binding energy.[18] For $n=13-16$ the interaction energies of H_2O are less than about 0.20 eV and there is no significant difference with a change in n. It increases a little from $n=13$ to $n=14$, as also discussed above, and then decreases again. In experiments, a little adsorption has been found only in $n=13$ and 14 and there is also a little increase in going from 13 to 14.

From the above, it is therefore clear that our results are in excellent agreement with reported experiments and show that H_2O adsorption could occur up to $n=12$. The experimental results also show some interesting behavior of the reaction ratio, which agrees completely with our calculations. First, the experimental ratio decreases in going from $n=7$ to $n=12$, with the value changing from 0.8 to 0.4. Besides the small decrease in the interaction energy that we obtained in our calculations (Fig. 3), the structure is also likely to play an important role in adsorption. The most favorable structures of $TiSi_n$ ($n=8-12$) are basket structures and with the increase in size, Ti atom loses its exposed part more and more, and finally at $n=12$, half of Ti is completely surrounded by Si atoms. Therefore, in such a structure, adsorption sites for H_2O become more limited so that the reaction ratio could decrease more significantly. The second interesting point is that in the experiment $n=13$ and 14 have still some reaction, while from $n=15$ the adsorption ratio is almost zero. As seen in Fig. 3, the inertness for adsorption is the same in $n=13-16$. However, considering the large structural change between $n=12$ and 13, the basket isomer for $n=13$ and 14 could exist even though cage isomer has an energetic advantage. The third interesting aspect is seen in $n=14$, which has larger adsorption ratio as compared to $n=13$. Our calculated results also show a slight increase in the interaction energy and this is likely to be responsible for an increase in the reaction ratio. In addition, $n=14$ cage isomer has two open hexagonal rings, while $n=13$ has one. A similar slight increase of the interaction ratio is seen for $n=10$ and there is a corresponding increase in the interaction energy as well.

$n=13-16$ clusters also have large highest occupied-lowest unoccupied molecular orbital gaps (more than 1.4 eV) and for $n=15$ and 16, it has values of 1.58 and 2.36 eV, respectively. This is also likely to be the reason for their inertness.

The bonding nature between $TiSi_n$ and H_2O is important to understand adsorption behavior of H_2O molecules. To analyze the interaction we have plotted the electronic-charge density distributions in Fig. 4 for $n=12$ and 13 as representative examples of the adsorbing and not-adsorbing clusters, respectively. For $n=12$ we have shown the total, excess, and depletion of charge with the excess and depletion charges defined as the differences between the interacting system $TiSi_n+H_2O$ and the sum of charges of the isolated $TiSi_n$ cluster and the H_2O molecule. From the total charge density distribution one finds strong covalent-like Si-Si bonds and some charge accumulation between Ti and H_2O. There is a small charge transfer from the vicinity of Ti and H ions to the region between the Ti and O ions. This charge transfer occurs in quite limited space so that the stability and the atomic structure of $TiSi_n$ cluster is not affected significantly. For $n=13$ we have shown only the total charge density distribution as the excess and depletion charge distributions are too small (less than 0.01 e/Å^3). Therefore, the charge transfer as well as the interaction between $TiSi_n$ cluster and H_2O molecule is rather weak, as expected.

The above description of interaction of water is corroborated by the orbital energies shown in Fig. 5. As one can see, the orbital energies of the $TiSi_{12}$ cluster get shifted upwards, while those of H_2O molecule shift significantly to higher binding energies indicating significant covalent bonding between water and the silicon cluster. On the other hand for $TiSi_{13}$, this shift is quite small, supporting the weak interaction.

In summary, we have reported *ab initio* calculations of the adsorption of a H_2O molecule on titanium-doped silicon clusters of different sizes. The equilibrium structures and interaction energies have been obtained. It is found that $TiSi_n$ clusters form a cage structure from $n=13$ onwards so that H_2O adsorption could occur only up to $n=12$, for which basket structures are preferred with Ti partially exposed and being available for interaction. These results are in excellent agreement with reported experimental results in which a little adsorption can be found beyond $n=12$. The interaction between $TiSi_n$ and H_2O is evaluated by the calculation of the interaction energy. It clearly shows a decrease from $n=12$ to $n=13$ and very small interaction energies for $n=14-16$, supporting their inertness and cage structures, in complete agreement with experiments.

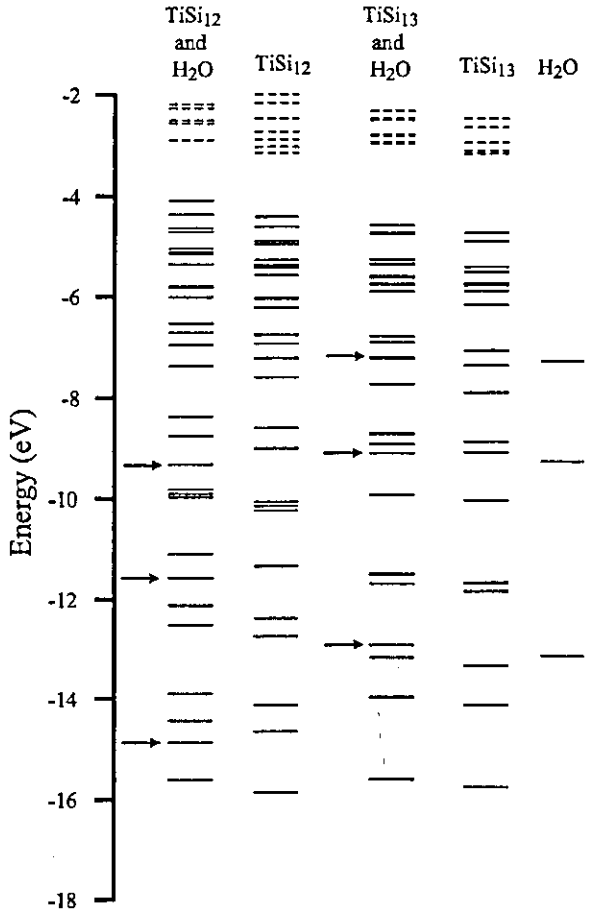

FIG. 5. Electronic levels for $TiSi_n$ ($n=12$ and 13) before and after interaction with H_2O and the H_2O molecule. Broken lines show the unoccupied levels. The arrows show the position of the H_2O levels after adsorption.

V.K. thankfully acknowledges the kind hospitality at the Institute for Materials Research and the support from JSPS. We are grateful to the staff of the Center for Computational Materials Science at IMR for making Hitachi SR8000 supercomputer available.

[1] V. Kumar and Y. Kawazoe, Phys. Rev. Lett. **87**, 045503 (2001); **91**, 199901 (2003); V. Kumar, Eur. Phys. J. D **24**, 227 (2003); V. Kumar, Comput. Mater. Sci. **30**, 260 (2004).
[2] V. Kumar and Y. Kawazoe, Phys. Rev. B **65**, 073404 (2002); V. Kumar and Y. Kawazoe, Appl. Phys. Lett. **83**, 2677 (2003); V. Kumar *et al.*, Nano Lett. **4**, 677 (2004).
[3] V. Kumar and Y. Kawazoe, Phys. Rev. Lett. **90**, 055502 (2003).
[4] S. N. Khanna *et al.*, Phys. Rev. Lett. **89**, 016803 (2002).
[5] S. N. Khanna *et al.*, Chem. Phys. Lett. **373**, 433 (2003).
[6] G. Mpourmpakis *et al.*, Phys. Rev. B **68**, 125407 (2003).
[7] J. Lu and S. Nagase, Phys. Rev. Lett. **90**, 115506 (2003).
[8] F. Hagelberg *et al.*, Phys. Rev. B **67**, 035426 (2003).
[9] P. Sen and L. Mitas, Phys. Rev. B **68**, 155404 (2003).
[10] G. Mpourmpakis *et al.*, J. Chem. Phys. **119**, 7498 (2003).
[11] S. M. Beck, J. Chem. Phys. **90**, 6306 (1989).
[12] H. Hiura *et al.*, Phys. Rev. Lett. **86**, 1733 (2001).
[13] V. Kumar *et al.*, Phys. Rev. B **68**, 155412 (2003).
[14] M. Ohara *et al.*, Chem. Phys. Lett. **371**, 490 (2003).
[15] G. Kresse and J. Furthmüller, Phys. Rev. B **54**, 11169 (1996); G. Kresse and J. Hafner, J. Phys.: Condens. Matter **6**, 8245 (1994).
[16] D. Vanderbilt, Phys. Rev. B **41**, 7892 (1990).
[17] J. P. Perdew and Y. Wang, Phys. Rev. B **45**, 13244 (1992).
[18] H. Kawamura, V. Kumar, and Y. Kawazoe, Phys. Rev. B (to be published).

Reprinted from

PHYSICAL REVIEW B

CONDENSED MATTER AND MATERIALS PHYSICS

NOVEMBER 2004
15(I)

Nonicosahedral growth and magnetic behavior of rhodium clusters

Young-Cho Bae,[1] Hiroki Osanai,[1] Vijay Kumar,[2,3] and Yoshiyuki Kawazoe[2]
[1]*CODEC Co., Ltd., Kawasaki 215-0033, Japan*
[2]*Institute for Materials Research, Tohoku University, Aoba-ku, Sendai 980-8577, Japan*
[3]*Dr. Vijay Kumar Foundation, 45 Bazaar Street, K. K. Nagar (West), Chennai 600 078, India*

Published by
THE AMERICAN PHYSICAL SOCIETY

Volume 70 Third Series Number 19

Nonicosahedral growth and magnetic behavior of rhodium clusters

Young-Cho Bae,[1] Hiroki Osanai,[1] Vijay Kumar,[2,3] and Yoshiyuki Kawazoe[2]
[1]*CODEC Co., Ltd., Kawasaki 215-0033, Japan*
[2]*Institute for Materials Research, Tohoku University, Aoba-ku, Sendai 980-8577, Japan*
[3]*Dr. Vijay Kumar Foundation, 45 Bazaar Street, K. K. Nagar (West), Chennai 600 078, India*
(Received 1 June 2004; revised manuscript received 23 July 2004; published 11 November 2004)

Ab initio pseudopotential calculations of the atomic structures and magnetic behavior of Rh_n ($n \leq 15$) clusters using the generalized gradient approximation for the exchange-correlation energy, reveal new lowest energy structures that are noncompact and have no atom at the center upto $n=13$, leading to a nonicosahedral growth. An eight-atom cluster has cubic structure and is magic. Some clusters beyond 13 atoms also do not have close packed structures due to some covalent character in the bonding. The calculated magnetic moments are generally lower and in better agreement with experiments than obtained before. Further studies on Ru_{13} and Pd_{13} clusters show that the lowest energy isomers of these clusters are also nonicosahedral. These findings of the novel behavior of technologically important transition metal clusters provide new ground for a better understanding and design of new catalysts.

DOI: 10.1103/PhysRevB.70.195413 PACS number(s): 36.40.Cg

I. INTRODUCTION

The occurrence of magnetism in clusters of nonmagnetic elements[1,2] Ru, Rh, and Pd has attracted much attention in recent years[3–8] but it is still not well understood. These elements lie in the periodic table just below the magnetic elements Fe, Co, and Ni, respectively, whose clusters have been found[9] to have enhanced magnetic moments as compared to bulk due to reduced coordination of atoms and localization of electrons. Such an enhancement in magnetic moments also occurs on surfaces[10] of magnetic elements where the coordination of atoms is again lower than in the bulk. The magnetic moments in these cases lie in between the values for the atom and the bulk. In clusters also, a large fraction of atoms lie on the surface and this leads to the development of magnetic moments in Ru, Rh, and Pd clusters. Earlier studies[3–7] on clusters of these elements overestimated the magnetic moments as compared to the measured values[1] and obtained an icosahedral growth. However, here we report the finding of nonicosahedral growth in Rh clusters. These isomers generally have lower magnetic moments as compared to those reported before leading to a better agreement with experiments.

In addition to the fundamental interest in magnetism and bonding nature as well as their correlation with the atomic structures of nanoclusters, Rh clusters are important for catalysis[11] and it is necessary to know the atomic structures and magnetic properties properly to understand their role in reactions. Experiments[1] in the temperature range of 60–300 K suggest Rh_n clusters to be magnetic upto about $n=60$ with a value of $0.48 \pm 0.13 \mu_B$/atom for Rh_{13}. *Ab initio* calculations have been done mostly on clusters having upto about 13 atoms. Studies using a tight binding model[8] on clusters with n upto about 200 also showed icosahedral isomers to be lowest in energy. A spin-polarized density functional study[3,4] of Ru, Rh, and Pd clusters having upto 147 atoms showed large magnetic moments on small clusters and icosahedral growth to be lowest in energy. For Ru and Rh the magnetic moments were found to decrease much faster as compared to Pd with an increase in the cluster size. The magnetic moment on Rh_{13} in an icosahedral structure has been calculated to be 1.62 and $1.15 \mu_B$/atom, respectively, by Reddy *et al.*[5] and Reddy *et al.*[6] Jinlong *et al.*[7] also obtained $15 \mu_B$ magnetic moment on Rh_{13} using the discrete variational method while Kumar and Kawazoe[4] obtained $21 \mu_B$ magnetic moment on this cluster. However, it was shown[4] that isomers with lower magnetic moments such as the one with $15 \mu_B$ lie only about 0.04 eV higher in energy and therefore lower magnetic moment isomers are expected to be present in experimental conditions. These results generally show that the calculated values are significantly higher than those obtained from experiments. Reddy *et al.*,[6] obtained structures using a parametrized model potential without spin polarization. The resulting structures were reoptimized using density functional calculations. Guirado-Lopez *et al.*[8] kept the symmetry of the clusters fixed. Our *ab initio* calculations surprisingly reveal noncompact and nonicosahedral structures to be energetically more favorable opening a new possibility in the understanding of this important class of clusters. A non-icosahedral growth has also been obtained[12] for Nb clusters. Therefore, we performed further checks on the structures of Ru_{13} and Pd_{13} clusters. Interestingly we find an icosahedron for Ru_{13} to be much higher in energy as compared to the non-compact structure while for Pd_{13} the noncompact structure is lower in energy but it is nearly degenerate with an icosahedron.

II. METHOD

The calculations have been performed using the *ab initio* ultrasoft pseudopotential plane wave method.[13,14] The cutoff energy for the plane wave expansion is taken to be 205.5, 203.6, and 199 eV for Rh, Ru and Pd, respectively. The generalized gradient approximation (GGA)[15] with spin polarization has been used for the exchange-correlation energy and the Γ point, for the Brillouin zone integrations. Several structures have been fully optimized using the conjugate gradient

 ©2004 The American Physical Society

method such that the force on each ion became less than 0.005 eV/Å. The energy is converged to an accuracy of 0.0001 eV. In most cases the low lying isomers are further checked for different spin-isomers using a constraint on the net magnetic moment and the reoptimization of the atomic structure. The binding energy (BE) of Rh_2 is calculated to be 2.04 eV/atom with the bond length of 2.20 Å. The magnetic moment reduces to $2\mu_B$/atom from the atomic value of $3\mu_B$. There is a large scatter in the available theoretical values for a dimer. We compare our results with those obtained by using GGA. Our BE (bond length) is slightly higher (shorter) as compared to 1.88 eV/atom (2.34 Å) obtained[6] by using DMOL and GGA. Also our BE is higher than the experimental value[16] of 1.46 eV/atom but the bond length is in better agreement with the experimental value of 2.28 Å. The bulk cohesive energy and lattice constant for Rh are calculated to be 6.06 eV/atom and 3.83 Å that are in good agreement with the experimental values of 5.75 eV/atom and 3.80 Å, respectively. Therefore, we expect a better prediction of the BEs of clusters with increasing size but an overall slight overestimation.

III. RESULTS

A. Structures

The low lying isomers of Rh_n clusters with $n=4-12$ are shown in Fig. 1. The BEs, magnetic moments, and mean nearest neighbor bond lengths of the lowest energy isomers are given in Table I. Earlier studies[6,7] have reported a tetrahedral structure for Rh_4 with $4\mu_B$ magnetic moment. This is nearly degenerate with a nonmagnetic tetrahedral isomer. We find a bent (nearly 90°) rhombus (side 2.41 Å, angles 71.9° and 70.4°, and diagonals 2.78 and 2.83 Å) to be lowest in energy with $6\mu_B$ magnetic moment while a square (side 2.33 Å) lies 0.15 eV higher in energy with $4\mu_B$ magnetic moment. A tetrahedron (side 2.45 Å) lies 0.19 eV higher in energy and is nonmagnetic. This is the first result for transition metal clusters that an open structure has lowest energy. For Rh_5, we obtain a square pyramidal structure (bond lengths 2.42 Å in the base and 2.54 Å from vertex to base) with $5\mu_B$ magnetic moment to be 0.31 eV lower in energy than a trigonal bipyramid (bond lengths 2.65 Å in the base and 2.50 Å from vertex to base) that has $7\mu_B$ magnetic moment. A similar result was obtained earlier.[6] For Rh_6 a slightly distorted prism with mirror symmetry (bond length varying between 2.36 to 2.47 Å with the mean value of 2.43 Å) and an octahedron (bond length varying from 2.50 to 2.66 Å with the mean value of 2.54 Å) each with $6\mu_B$ magnetic moment are nearly degenerate while a bicapped tetrahedral structure lies 0.31 eV higher in energy with $10\mu_B$ magnetic moment. A nonmagnetic octahedral isomer lies only 0.05 eV higher in energy than the $6\mu_B$ isomer and therefore in this octahedral isomer the magnetic behavior is very weak and can be easily destroyed even at quite low temperatures. However, the nonmagnetic prism isomer lies 0.22 eV higher in energy and therefore it is unlikely to be observed at room temperature. An isomer with the capping of the lowest energy Rh_5 pyramid structure lies 0.55 eV higher in energy with $4\mu_B$ magnetic moment. We also calculated a planar triangular structure and a hexagon. These lie 2.08 and 3.38 eV higher in energy with 8 and $0\mu_B$ magnetic moments, respectively than the lowest energy isomer. Therefore, these low dimensional structures lie significantly higher in energy for $n=6$. Earlier an octahedral structure was obtained for this cluster. However, our finding of the prism structure is important as for Rh_7 also we find a square capped prism structure with $11\mu_B$ magnetic moment to be 0.12 eV lower in energy than a pentagonal bipyramid ($13\mu_B$) obtained before.[6,7] An isomer in which a triangular face of the prism is capped lies 0.48 eV higher in energy with $7\mu_B$ magnetic moment.

Another surprising finding is that Rh_8 has a perfect cubic structure with 2.40 Å side and $12\mu_B$ magnetic moment. The bond length is quite short and it reflects the strong covalent bonding in this cluster. It lies about 1 eV lower in energy

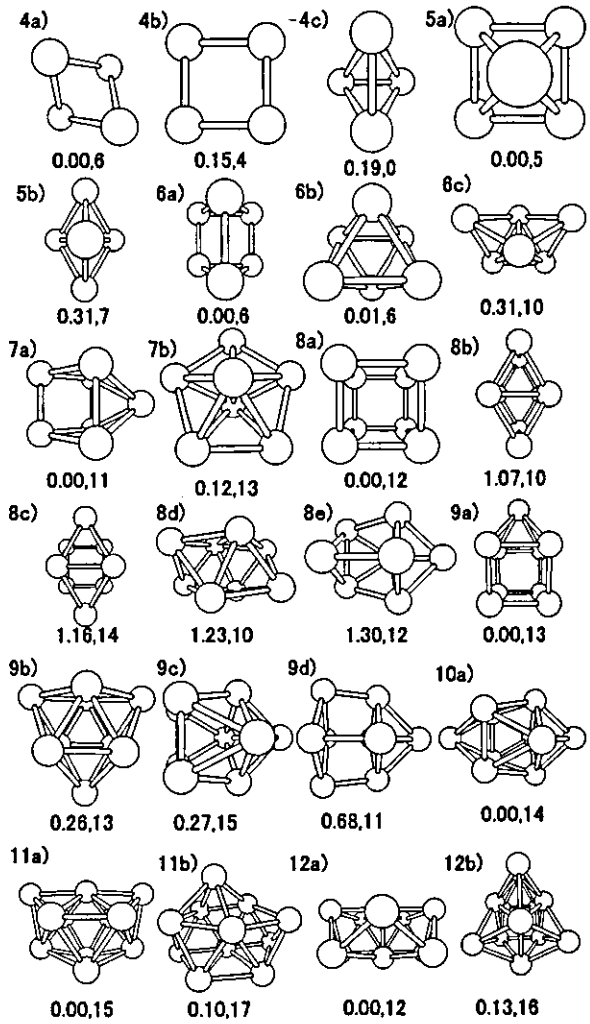

FIG. 1. Atomic structures of Rh_n clusters with $n=4-12$. Isomer (a) has the lowest evergy which is taken as reference. The relative energies (eV) of other isomers are given below each structure along with the magnetic moment in the unit of μ_B. The structure of 12a has six atoms in each layer. There is one atom in the center of the upper layer to which two side atoms are connected. The front atom in this layer is connected with two atoms in the lower layer. The latter also has one atom behind the central atom. The smaller the size of the ball, the deeper is the position.

TABLE I. The binding energy (BE), magnetic moment (M), and mean nearest neighbor bond lengths (d) in the lowest energy isomers of Rh clusters.

n	Structure	BE (eV/atom)	M (μ_B)	d (Å)
4	Bent rhombus	3.12	6	2.41
5	Square pyramid	3.40	5	2.48
6	Prism	3.57	6	2.43
7	Capped prism	3.71	11	2.50
8	Cube	3.96	12	2.40
9	Capped cube	3.97	13	2.47
10	Bicapped tetragonal antiprism	4.02	14	2.56
11	Fused pentagonal pyramids	4.06	15	2.57
12	Bilayers	4.12	12	2.55
13	Cage	4.16	17	2.57
14	capped hexagonal prism-like	4.23	16	2.55
15	Hexagonal	4.26	19	2.62

than many other isomers [8(b)–8(e) in Fig. 1] such as two prisms fused on a square face, a bicapped prism, a D_{2d} type structure, and a capped pentagonal bipyramid that are 1.07, 1.16, 1.23, and 1.30 eV higher in energy with 10, 14, 10, and $12\mu_B$ magnetic moments, respectively. As we shall show later, this cluster shows magic behavior. Among transition metal clusters, eight-atom cluster of Nb has also been found[12] to be magic but the lowest energy structure of Nb_8 is a bicapped octahedron. These results indicate that the close packed structures of Rh clusters are not of the lowest energy and the growth behavior in this size range does not follow the partial icosahedral structure route. In fact the capped pentagonal bipyramid structure lies highest in energy among these isomers. Furthermore a tetrahedron with four faces capped and a hexagonal bipyramid of Rh_8 lie 2.09 and 2.92 eV higher in energy with 12 and $0\mu_B$ magnetic moments, respectively.

The above growth behavior is continued further and Rh_9 is a capping of cubic Rh_8 with $13\mu_B$ magnetic moments. It is quite different from a bicapped pentagonal bipyramid obtained earlier.[6] We obtain a capped tetragonal antiprism (9c) to be 0.27 eV higher in energy. It has $15\mu_B$ magnetic moment. This can also be considered as a pentagonal prism capped with a triangle on one side. A capped tetragonal prism type isomer (9d) lies 0.68 eV higher in energy and is unlikely to be present in experiments. We also obtained a tricapped prism (9b) which is 0.26 eV higher in energy and has $13\mu_B$ magnetic moments. Therefore, our results are the lowest spin isomers. However, for Rh_{10}, our result of bicapped tetragonal antiprism (10a) ($14\mu_B$ magnetic moments) is the same as obtained before.[7] A bicapped distorted hexagonal biprism lies 0.30 eV higher in energy with $16\mu_B$ magnetic moments whereas a bicapped (opposite faces) cube and two interconnected pentagonal bipyramids lie significantly higher (0.95 and 1.19 eV) in energy with 10 and $12\mu_B$ magnetic moments, respectively. Several different cappings of a pentagonal bipyramid were also optimized and these lie 0.5 eV or higher in energy, supporting the non-icosahedral growth in these clusters.

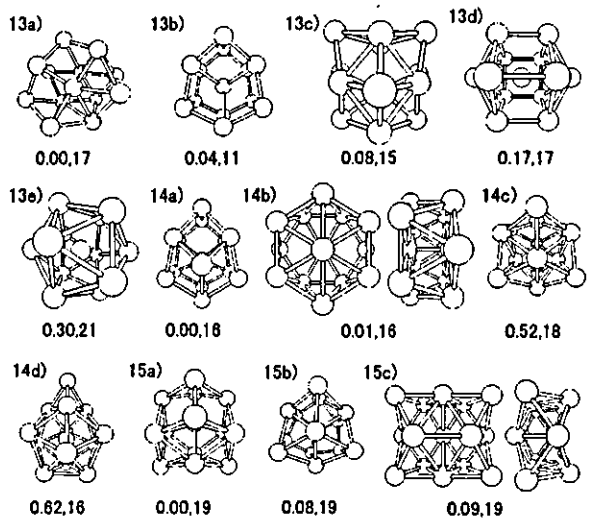

FIG. 2. The same as in Fig. 1 but for $n=13-15$.

The lowest energy isomer of Rh_{11} (11a) can be viewed as two capped pentagons joined by an atom. It has $15\mu_B$ magnetic moments. Another low lying isomer (11b) can be viewed as capped two layers of five atoms each (five atoms in a triangular packing in one layer and a pentagon in another). It lies only 0.10 eV higher in energy and has $17\mu_B$ magnetic moments. It is likely to be present in experiments. This structure is a precursor to the lowest energy structures of Rh_{12} and Rh_{13}. There is no atom at the center. Similarly for $n=12$, a two layer structure (12a) has the lowest energy. It has mirror symmetry and $12\mu_B$ magnetic moments. Increasing or decreasing the magnetic moments of this cluster by $2\mu_B$ makes only a small change in energy of about 0.1 eV and therefore, the magnetic moments can be easily affected by temperature. There are slightly different isomers. One is shown in Fig. 1 (12b) and it lies only 0.13 eV higher in energy and should also be present in experiments. It also has a mirror symmetry with the magnetic moments of $16\mu_B$. So in this case, it can be possible that there is an increase in the magnetic moments with an increase in temperature.

The most important result is obtained for Rh_{13}. Earlier an icosahedron has been reported to be lowest in energy.[4–7]. We carried out optimizations for icosahedron, cuboctahedron, decahedron, and capped cubic structures as well as several other isomers. A few low lying isomers are shown in Fig. 2. Surprisingly a cage structure (13a) with $17\mu_B$ magnetic moment and no atom at the center is 0.30 eV lower in energy than an icosahedron (13e) with $21\mu_B$ magnetic moment as obtained before.[4] (An icosahedral isomer with $17\mu_B$ magnetic moment is only about 0.01 eV higher in energy and is almost degenerate.) It has a pentagon (in the middle), a rhombus on one side, and a near square on the other. These results indicate that in general, Rh clusters prefer relatively open structures. Several other atomic and spin isomers lie close in energy. This will also lead, in general, to spin isomers with lower magnetic moments to be present in experiments. There is an isomer (with mirror symmetry) (13b)

which is only 0.04 eV higher in energy and has $11\mu_B$ magnetic moments. This will be also abundant in experimental conditions and will give rise to an average lower magnetic moment on this cluster and therefore a better agreement with the experimental[1] value of $0.48\pm0.13\mu_B$/atom. This is in contrast to the value of $1.62\mu_B$/atom obtained by Reddy *et al.*[5] using the local density functional theory while Jinlong *et al.* as well as Reddy *et al.*[6] obtained $1.15\mu_B$/atom for this cluster. As we shall show later, there is some directionality in bonding in isomer (13b). This is also seen from the fact that a nearly hexagonal prism isomer with an atom at the center lies 0.44 eV higher in energy with $15\mu_B$ magnetic moment than isomer (13b). The latter is important as Rh_{14} is obtained from it. We also show two more isomers (13c and 13d) that are 0.08 eV [with $15\mu_B$ magnetic moments and somewhat similar to (13a)] and 0.17 eV (decahedral with $17\mu_B$ magnetic moment) higher in energy than the isomer (13a). Many other isomers were also studied but these are higher in energy.

A few optimized structures for Rh_{14} are shown in Fig. 2. The lowest energy isomer of Rh_{14} is obtained from isomer (13b) by capping a hexagonal face. It has $16\mu_B$ magnetic moments. A hexagonal anti-prism with each hexagon having an atom at the center (14b) is nearly degenerate with $16\mu_B$ magnetic moments. In this case there is no atom at the center. Another isomer with three-fold symmetry and no atom at the center (14c) lies 0.52 eV higher in energy with $18\mu_B$ magnetic moments. A capped icosahedron (14d) lies 0.62 eV higher in energy, again showing that icosahedral growth is not favored. A cubic isomer with capping of the six faces lies 0.52 eV higher in energy and has $18\mu_B$ magnetic moments. The lowest energy structure of Rh_{15} is derived from the lowest energy isomer of Rh_{13}. It has an atom at the center of a bent hexagon with a tetramer on either side and $19\mu_B$ magnetic moments. There are several other isomers that have lower or equal magnetic moments and which will be present in experiments below room temperature and give rise to a lower estimation of the magnetic moments on this cluster. Two such isomers are shown in Fig. 2. The isomer (15b) is derived from (14a) with both hexagonal (the six atoms are not in a plane) faces capped while (15c) has two layers with no atom at the center. These results show that relatively open (noncompact structures) are more favored by Rh clusters. Some of the properties of the lowest energy isomers of $n=13-15$ clusters are given in Table I.

In general we find an abundance of rhombii in the lowest energy structures of Rh clusters. Starting from Rh_4, one can consider the growth process to follow from addition of an atom to an existing cluster with significant relaxations. This way one can account for the growth upto $n=10$. Rh_{11} can be considered to be a symmetrical capping by two atoms on a Rh_9 cluster having a capped tetragonal antiprism structure. However, the capped tetragonal antiprism isomer of Rh_9 lies significantly higher in energy. So the growth process can be quite complex and in the cases where more than one isomer are nearly degenerate, there could be different routes for the growth of these clusters.

B. Cagelike structure

The result that icosahedron is not of the lowest energy for Rh_{13} and that a relatively open cage structure has lower energy is significant in understanding the growth behavior of transition metal clusters. In fact non-icosahedral growth was also reported earlier[12] for Nb clusters. In order to check if a similar behavior would be found in clusters of Pd and Ru that are neighboring elements to Rh in the periodic table, we performed calculations for Pd_{13} and Ru_{13}. It is found that in these cases also an icosahedron is not of the lowest energy. For Ru_{13} the second best isomer (13b) of Rh_{13} has the lowest energy with $4\mu_B$ magnetic moments while the one with the structure of the best isomer (13a) of Rh_{13} lies 1.56 eV higher in energy with $2\mu_B$ magnetic moments. Changing the spin in these isomers costs little energy (see Fig. 3 for Rh clusters) and therefore the magnetic moments can be easily supressed in these clusters. The icosahedral isomer lies 2.25 eV higher in energy and has a large magnetic moment of $12\mu_B$. Therefore icosahedral structure is very unfavorable for Ru and our results explain the nearly nonmagnetic behavior found in these clusters in experiments.[1] For Pd_{13} the best structure of Rh_{13} also has the lowest energy with $8\mu_B$ magnetic moments but an icosahedral isomer reported earlier[3] lies only 0.05 eV higher in energy with $8\mu_B$ magnetic moment. Therefore for Pd_{13} these two isomers are nearly degenerate. The bonding in

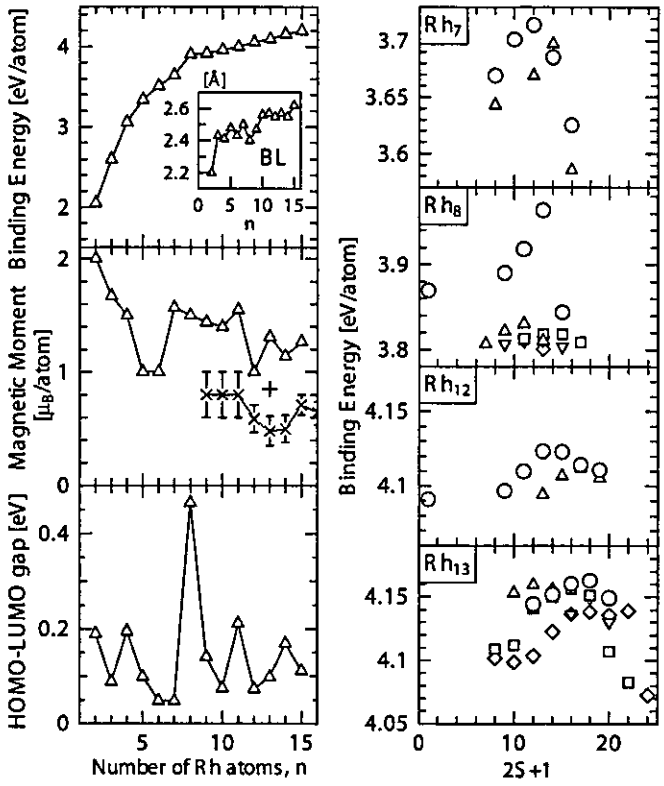

FIG. 3. Binding energies, magnetic moments, and HOMO-LUMO gaps of Rh_n clusters are plotted in the left panel. A plus (+) shows the magnetic moment of the isomer (13b) which gives a much better agreement with the overall trend found in experimental results which are shown by crosses with error bars. Inset shows the mean nearest neighbor bond lengths. The energies of the spin isomers are shown for $n=7$, 8, 12, and 13 in the right panel. S equals half the value of the total magnetic moment. Circles, triangles, squares, reverse triangles, and diamonds represent, respectively, the isomers (a)–(e) in Figs. 1 and 2.

Pd clusters is much weaker as delocalization of $4d$ electrons occurs slowly and this could explain why icosahedral structure becomes more favorable in Pd. The lowest energy isomer of Ru_{13} [(13b) in Fig. 2] lies 0.81 eV higher in energy for Pd and has $6\mu_B$ magnetic moments. Therefore, the behaviors of Pd and Ru clusters are quite different. A decahedron of Pd_{13} lies 0.34 eV higher in energy and has $8\mu_B$ magnetic moments. These results show that Pd_{13} has the same magnetic moments in quite different structures.

C. Calculated properties

The BE is shown in Fig. 3 for the lowest energy isomers of Rh clusters. It increases monotonically as the cluster size increases and has a small peak at $n=8$. Interestingly there is also a significant highest occupied-lowest unoccupied molecular orbital (HOMO-LUMO) gap for Rh_8 making it behave like a magic cluster. In most of the other clusters the HOMO-LUMO gap is generally small and shows an oscillatory behavior. There is an overall decrease with an increase in size. This is expected as bulk Rh is a metal. The magnetic moments per Rh atom (Fig. 3) show an oscillatory behavior as a function of the cluster size but overall there is a decreasing trend as the bulk is nonmagnetic. The magnetic moment is nearly constant in the range of $n=7-11$ and for $n=12$ there is a significant drop. These results agree well with the experimental data[1] that show $0.8\pm0.2\mu_B$/atom magnetic moment for $n=9-11$ and then $0.59\pm0.12\mu_B$/atom for $n=12$. Also our result of $0.85\mu_B$/atom magnetic moment for the isomer (13b) agrees well with an experimental decrease in the magnetic moment from $n=12$ to 13 and then for $n=14$ and 15, there is an increase in the magnetic moment again in agreement with the trend found in experiments (experimetal values being 0.50 ± 0.12 and $0.71\pm0.09\mu_B$/atom for $n=14$ and 15, respectively). The overall good agreement with the experimetal results gives us confidence that our calculated lowest energy structures are close to the experimental findings. The experimetal values of the magnetic moments are nearly uniformly lower and this could be due to the fact that theoretical results are at zero temperature while experimental results correspond to temperatures in the range of 60–300 K. We have also shown the variation in the energy of the spin isomers considering the cases of clusters with $n=7$, 8, 12, and 13. This is generally small as the total spin is changed to a lower value while the energy decreases more sharply for higher spin isomers. As mentioned before, this could account for the observed lower magnetic moments because isomers with lower magnetic moments would also be present. Our finding of a new isomer of $n=13$ is particularly noteworthy and this could explain the much lower magnetic moments observed for Rh_{13}.

It is worth to point out here that in our studies we have ignored orbital contribution to the magnetic moments. In recent years there are efforts[17] to include the orbital contribution as well as the magnetic anisotropy in clusters. The orbital contribution would increase the total magnetic moment and therefore would lead to a larger difference with the experimental results. Guirado-Lopez *et al.*[18] have calculated the orbital magnetic moments for Rh clusters using a self-consistent tight-binding method and representative face center cubic structures with bulk nearest neighbor bond lengths. The average orbital magnetic moments have been reported to lie in the range of $0.1-0.24\mu_B$/atom for $n\leq19$ with strong oscillations as a function of n. The orbital contribution to the magnetic moments is expected to be sensitive to the structures of clusters and as our results show, the structures of Rh clusters are generally very different from the high symmetry structures considered by these authors. We shall expect that the significantly lower symmetry in most cases of Rh clusters would lead to a reduced contribution from orbital magnetic moments. Further, in order to find a correlation between the magnetic moments and the bond lengths or the coordination number, we calculated the local magnetic moments around each ion for a few clusters. However, we do not find a systematic trend. In general a higher coordination or a short bond length reduces magnetic moments due to the increased hybridization. This can be seen from the lowest energy isomer of Rh_6. In this isomer there is one bond which is shortest (2.36 Å) and the local magnetic moments on the two atoms are the smallest ($\approx0.8\mu_B$) while on the remaining atoms the magnetic moments are $\approx1.1\mu_B$. In this case the coordination of each atom is 3 and therefore the short bond is responsible for the reduced moment. However, in the case of the lowest energy isomer of Rh_{13}, an atom with coordination 7 has magnetic moments of $0.97\mu_B$, whereas the other two atoms with coordination 7 have 1.45 and $1.17\mu_B$ magnetic moments. Therefore, there does not appear to be a straightforward correlation with the coordination number. Similarly in the case of the lowest energy isomer of Rh_{11}, most of the atoms have coordination 5 and two atoms have coordination 4 while one atom has coordination 6. In this case the local magnetic moments have values lying in between 1.22 and $1.59\mu_B$. Atoms with coordination 4 are symmetrically located and have $1.22\mu_B$ magnetic moments while two symmetrically placed atoms with coordination 5 have the highest local magnetic moments of $1.59\mu_B$. An atom with coordination 6 has the local magnetic moments of $1.44\mu_B$. Further calculations on Rh_{14} show that an atom with coordination 3 has the highest magnetic moment of $1.39\mu_B$. For this atom the nearest neighbor bond lengths have values of about 2.61, 2.61, and 2.65 Å while a few other atoms with coordination ranging from 3 to 5 have reduced local magnetic moments of about $1.02\mu_B$ due to the short nearest neighbor bonds of about 2.44 Å. The atom with the highest coordination of 8 has the local magnetic moment of $1.08\mu_B$. We also studied the local moments in the case of the lowest energy isomer of Rh_{15}. Two symmetrically placed atoms with coordination 6 have the lowest local magnetic moments of $0.98\mu_B$ while the atom at the center with coordination 8 has the local magnetic moments of $1.05\mu_B$. On other atoms the local magnetic moments lie in the range of $1.23-1.41\mu_B$ though the coordination changes from 3 to 5. These results show the complex nature of the magnetic moments in these clusters, though in all cases we obtain ferromagnetic coupling.

The calculated mean bond lengths for Rh clusters are shown in the inset of Fig. 3 and the values are also given in Table I. For small clusters there is significant contraction and the bond length approaches towards the calculated bulk value (2.71 Å) in an oscillatory manner. Rh_8 has short bond

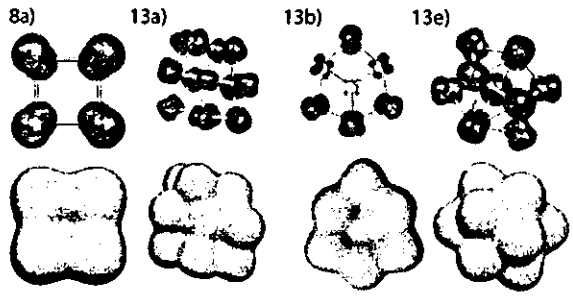

FIG. 4. (Color online) Spin-polarization (upper) and isosurfaces (lower) of the total charge density for isomers (8a), (13a), (13b), and (13e).

lengths which have the lowest value after $n=2$. Also in some clusters such as isomer (13b), there are many short bonds [bond lengths 2.39, 2.41, 2.44, 2.46 Å as compared to the mean bond length of 2.57 Å in isomer (13a)] which indicate directional bonding and covalent character in these clusters. We also calculated the mean coordination in these clusters and for the lowest energy isomers of Rh_n with $n=4-15$, the values are 2, 3.2, 3, 3.71, 3, 3.56, 4.8, 4.91, 4.67, 4.92, 4.14, and 4.67. Some clusters have low mean coordination such as $n=8$ and 14. Also the second lowest energy isomer of $n=13$ has the mean coordination of 3.69. These reflect covalent character of bonding in these clusters. It is more clearly seen from the isosurfaces of the magnetic polarization and the charge densities shown in Fig. 4 for a few selected isomers of Rh_{13} and the lowest energy isomer of Rh_8. In the case of isomers (13a) and (13e) the polarization is nearly uniformly distributed over the whole cluster, while in the case of the isomer (13b) the central atom and four atoms at the surface of the cluster have much less polarization than the rest of the atoms. These atoms have higher coordination. The bond lengths are short (2.51 Å) with four symmetic atoms and 2.58 Å with two atoms from the center) but not the shortest. The central atom has the highest coordination and the lowest polarization. So a higher coordination reduces the magnetic moments significantly but short bond lengths are also responsible for much reduced magnetic moments in this cluster. This leads to much more hybridization between the *sp-d* states which is also seen from the plots of the angular momentum decomposed density of states (Fig. 5). Also for the isomers (13a) and (13e) the charge densities are more uniformly distributed [though isomer (13a) appears to have some covalent character] while for isomer (13b), the covalent character is quite clear. In Rh_8 the charge density and polarization are symmetric reflecting the underlying symmetry of the cluster, but the directional bonding does not appear to be very strong. These results are important revelations of the nature of bonding and unexpected relatively open structures in clusters of these transition metals. The angular momentum decomposed and gaussian broadened densities of states show (Fig. 5) that the *sp-d* hybridization in the case of the isomer (13b) is more significant than in isomer (13a). Also the HOMO lies in a large gap in the up-spin states of the isomer (13a) though the other states are generally uniformly distributed due to the low symmetry of this cluster. On the other hand for the isomer (13b) the HOMO lies in a very small gap and there are many unoccupied states in the up-spin energy spectrum.

IV. SUMMARY

We have studied from first principles the atomic and electronic structures of small Rh clusters and found for the first time relatively open structures to be lower in energy than the icosahedral structures obtained before. In general these isomers have lower magnetic moments and this result is in better agreement with the available experimental data. In particular clusters with 13 or less number of atoms have no atom at the center. Though an atom goes at the center for clusters having more than 13 atoms, the structures are not the closest packed. We find an isomer of 13-atom cluster which is nearly degenerate with the lowest energy isomer and has a

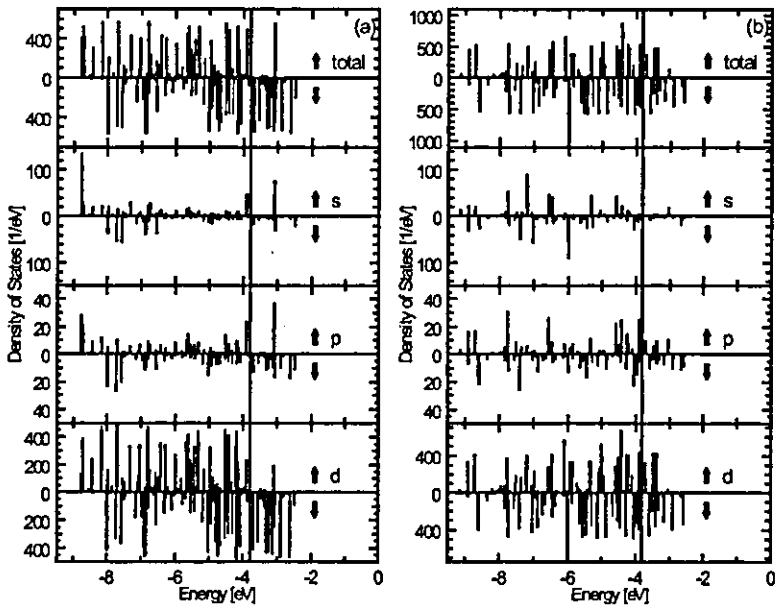

FIG. 5. Gaussian broadened total and angular momentum decomposed electronic states of (13a) and (13b) isomers. The vertical line shows the HOMO.

significantly lower magnetic moment. The latter is in better agreement with the experimental result. In general we find several isomers which lie close in energy and therefore, it is very likely that in experiments one has these isomers unless these are performed at very low temperatures. Our results also show that there is some covalent bonding character in these clusters that is responsible for the relatively open structures. Rh_8 is found to be magic. Further, our preliminary studies on Ru and Pd clusters show that similar structures are lower in energy for Ru clusters than those based on the icosahedral growth while for Pd clusters, the two growth modes may be nearly degenerate. Our results thus open a new chapter in the study of this important class of transition metal clusters. This would lead to a better understanding of the physicochemical properties of these clusters and reactions and to a better design of catalysts.

ACKNOWLEDGMENTS

The authors would like to thank the staff of the Center for Computational Materials Science of the Institute for Materials Research, Tohoku University for their continuous support of the supercomputing facility. V.K. thankfully acknowledges the kind hospitality at the IMR.

[1] A.J. Cox, J.G. Louderback, and L.A. Bloomfield, Phys. Rev. Lett. **71**, 923 (1993); A.J. Cox, J.G. Louderback, S.E. Aspeal, and L.A. Bloomfield, Phys. Rev. B **49**, 12 295 (1994).

[2] V. Kumar, K. Esfarjani, and Y. Kawazoe, in *Clusters and Nanomaterials*, edited by Y. Kawazoe, T. Kondow, and K. Ohno, Springer Series in Cluster Physics (Springer-Verlag, Heidelberg, 2002), p. 9.

[3] V. Kumar and Y. Kawazoe, Phys. Rev. B **66**, 144413 (2002).

[4] V. Kumar and Y. Kawazoe, Eur. Phys. J. D **24**, 81 (2003).

[5] B.V. Reddy, S.N. Khanna, and B.I. Dunlap, Phys. Rev. Lett. **70**, 3323 (1993).

[6] B.V. Reddy, S.K. Nayak, S.N. Khanna, B.K. Rao, and P. Jena, Phys. Rev. B **59**, 5214 (1999).

[7] Y. Jinlong, F. Toigo, and W. Kelin, Phys. Rev. B **50**, 7915 (1994).

[8] C. Barreteau, R. Guirado-Lopez, D. Spanjaard, M.C. Desjonqueres, and A.M. Oles, Phys. Rev. B **61**, 7781 (2000); R. Guirado-Lopez, M.C. Desjonqueres, and D. Spanjaard, *ibid.* **62**, 13 188 (2000).

[9] I.M.L. Bilas, A. Chatelian, and W.A. de Heer, Science **265**, 1682 (1994).

[10] O. Eriksson, A. M. Boring, R. C. Albers, G. W. Fernando, and B. R. Cooper, Phys. Rev. B **45**, 2868 (1992); M. Alden, S. Mirbt, H. L. Skriver, N. M. Rosengaard, and B. Johansson, *ibid.* **46**, 6303 (1992).

[11] J. Wei and E. Iglesia, J. Catal. **225**, 116 (2004).

[12] V. Kumar and Y. Kawazoe, Phys. Rev. B **65**, 125403 (2002).

[13] G. Kresse and J. Hafner, J. Phys.: Condens. Matter **6**, 8245 (1994).

[14] G. Kresse and J. Furthmüller, Phys. Rev. B **54**, 11 169 (1996); Comput. Mater. Sci. **6**, 15 (1996).

[15] J.P. Perdew, in *Electronic Structure of Solids*, edited by P. Ziesche and H. Eschrig (Akademie Verlag, Berlin, 1991).

[16] K.A. Gingerich and D.L. Cocke, J. Chem. Soc., Chem. Commun. **1**, 536 (1972).

[17] R. A. Guirado-Lopez, J. Dorantes-Davila, and G. M. Pastor, Phys. Rev. Lett. **90**, 226402 (2003); A. N. Andriotis and M. Menon, *ibid.* **93**, 026402 (2004); J.T. Lau, A. Föhlisch, R. Nietubyc, M. Reif, and W. Wurth, *ibid.* **89**, 057201 (2002); X. Wan, L. Zhou, J. Dong, T.K. Lee, and D.-S. Wang, Phys. Rev. B **69**, 174414 (2004).

[18] R. Guirado-Lopez, P. Villasenor-Gonzalez, J. Dorantes-Davila, and G.M. Pastor, Eur. Phys. J. D **24**, 73 (2003).

NANO LETTERS

2004
Vol. 4, No. 4
677−681

Smallest Magic Caged Clusters of Si, Ge, Sn, and Pb by Encapsulation of Transition Metal Atom

Vijay Kumar,*,†,‡ Abhishek Kumar Singh,† and Yoshiyuki Kawazoe†

Institute for Materials Research, Tohoku University, Sendai 980-8578, Japan, and Dr. Vijay Kumar Foundation, 45 Bazaar Street, K. K. Nagar (West), Chennai 600078, India

Received February 4, 2004; Revised Manuscript Received March 3, 2004

ABSTRACT

Ten atom clusters of X = Si, Ge, Sn, and Pb are known to be magic, suggesting that addition of an atom to such clusters is generally unfavorable. However, here we report using an ab initio ultrasoft pseudopotential method that these clusters can be further stabilized by doping of a Ni or Pt atom, leading to some of the smallest metal encapsulated clusters of these elements. For Si and Ge, doping of Ni is optimal while for Sn and Pb, Pt is the best. Our results agree with the recent observations of strong abundances and magic nature of $X_{10}Co^-$ clusters of these elements. These findings could lead to the development of novel cluster-based nanomaterials for optoelectronic and other nanoscale applications.

Clusters of semiconducting materials are currently of great interest as these have an important role to play not only in the miniaturization of devices but also in the fundamental understanding of materials at the nanoscale. Clusters with novel properties such as enhanced stability by suitable doping, tunable gaps, and magnetic properties could lead to novel nanoscale optoelectronic as well as miniature spintronic and storage devices. The recent findings[1−6] of metal (M) encapsulated clusters of Si and Ge have generated much interest in this field and could lead to new possibilities of Si- and Ge-based nanomaterials. The M encapsulated clusters can be very symmetric with much higher band gaps that lie in the visible region in some cases.[7] These properties may extend their usage in photonics that could be combined with electronics to lead to new optoelectronic devices. It has been further shown that these clusters could be assembled to form nanotubes[8−10] of Si and Ge with novel magnetic properties such as high magnetic moments and piezomagnetic effect[11] at the nanoscale. Following these findings, there is a growing interest[12−15] in the field of M encapsulated clusters and their nanotubes[16] in order to explore their properties as well as new possibilities both theoretically and experimentally.

Recently, anion binary clusters of Co/Ge, Co/Sn, and Co/Pb have been produced[17] by laser ablation with high abundance of $X_{10}M^-$ clusters followed by a minimum for $X_{11}M^-$. There is an extraordinary peak in the mass distribution for $Ge_{10}Co^-$. The ground state of these clusters is predicted[18] to be a bicapped tetragonal antiprism. However, why these clusters exhibit magic behavior with such a large abundance is not understood. Here we explain the unusual stability of these charged clusters and explore several binary combinations to predict new magic clusters of Si, Ge, Sn, and Pb with 10 atoms doped with Ni, Pd, or Pt. These are the smallest caged clusters of these elements doped with a transition (T) M atom. Si and Ge clusters are important for semiconductor devices while Sn and Pb are useful for soldering. Doping of M atoms provides a nice way to manipulate their properties at the nanoscale.

In $Ge_{10}Co$ anions Co atom can be replaced by the next element, namely Ni to obtain neutral clusters. As the size of the M atom plays an important role[1−3] in the stability and structures of M encapsulated Si or Ge clusters, we explore the optimal combinations among the TM and group-14 elements in order to find the most stable clusters. Si_{10}, Ge_{10}, Sn_{10}, and Pb_{10} are known to be magic with high abundances[17,19] and have compact structures[20] unlike the relatively open bulk diamond structure of Si, Ge, and Sn. All these clusters also have large highest occupied−lowest unoccupied molecular orbital (HOMO−LUMO) gaps (Table 1) that decrease in going from Si to Pb. Therefore, it would appear difficult to transform such magic clusters into other magic clusters by doping of an atom, as by definition of magic clusters, addition of one more atom of the constituent is less favorable. However, it is possible that a different isomer of

* Corresponding author. Vijay Kumar, Institute for Materials Research, Tohoku University, Katahira 2-1-1, Aoba-ku, Sendai 980-8577 Japan. Phone: 81-22-215-2287. Fax: 81-22-215-2052. E-mail: kumar@imr.edu.
† Tohoku University.
‡ Dr. Vijay Kumar Foundation.

10.1021/nl0498076 CCC: $27.50 © 2004 American Chemical Society
Published on Web 03/20/2004

Table 1. Binding Energies (BEs) and HOMO−LUMO Gaps of the Lowest Energy Isomers of X_{10} and M Doped Clusters

	BE (HOMO−LUMO gap) (eV)			
X	X_{10}	Ni	Pd	Pt
Si	3.85 (2.09)	3.95 (1.94)	3.81 (1.70)	3.94 (1.29)
Ge	3.35 (1.94)	3.55 (1.66)	3.34 (1.46)	3.52 (1.54)
Sn	2.91 (1.54)	3.15 (1.24)	3.06 (1.17)	3.24 (1.30)
Pb	2.69 (0.90)	2.92 (0.84)	2.86 (0.95)	3.04 (1.06)

the same cluster gets stabilized by doping. Recently, doping of Si, Ge, and Sn clusters with divalent M atoms was shown[21] to lead to such a behavior. In particular, Be doping enhances significantly the stability of the elemental magic clusters of these elements in a different structure and also changes some nonmagic clusters into magic ones. From the point of view of usage, Be is not favored because of its toxic nature. On the other hand, TM atoms are particularly important[7] for the stability of M encapsulated Si and Ge clusters. Therefore, the finding of large abundances of $X_{10}Co^-$ is significant. It is possible that the d level of the M atom is fully occupied and it behaves like the closed shell divalent M atoms. Therefore, the magic nature of the X_{10} cluster can be retained if the HOMO−LUMO gap remains significant.

$Ge_{10}Co^-$ has been shown[18] to have a large HOMO−LUMO gap, while we find that the neutral $Ge_{10}Co$ cluster has a significantly reduced gap of 0.23 eV only. For the stability of the neutral clusters it is important that these have large HOMO−LUMO gaps. The exceptional stability of $Ge_{10}Co^-$ and large HOMO−LUMO gap therefore arise due to the charged nature of these clusters. It is also noteworthy that cation $Ge_{10}Co$ does not show high abundance. For neutral clusters, we choose Ni as it has 10 valence electrons in $3d^94s^1$ configuration. In the doped cluster, it is possible that the 4s electron is transferred to the 3d level. If so, it is further important to find the optimal combination of TM atom in the same column and the group 14 elements.

The optimizations have been performed using an ab initio ultrasoft pseudopotential plane wave method[22] and the conjugate gradient technique with the generalized gradient approximation (GGA) for the exchange-correlation energy. The cutoff energy for the plane wave expansion is taken to be 17.76, 14.63, and 14.07 Ry for Ni, Pd, and Pt doped clusters, respectively. The Brillouin zone is represented by the Γ-point. The structures are considered to be converged when the force on each ion becomes 0.01 eV/Å or less. We consider a few initial structures such as the one with the M atom at the center of a tetracapped trigonal prism (TTP) (lowest energy structure[20] for X_{10}, X = Si, Ge, and Sn), a bicapped tetragonal antiprism (close to the lowest energy structure for Pb_{10}), a bicapped cube, a decahedron, a pentagonal antiprism, and outside doping of TTP to explore the lowest energy structures. In Table 1, we have given the binding energies (BEs) and HOMO−LUMO gaps of X_{10} and the M doped clusters in the lowest energy structures.

Figure 1 shows four typical structures that are among the lowest energy structures for these clusters. For $Si_{10}Ni$, the lowest energy structure is one with a capped pentagon on

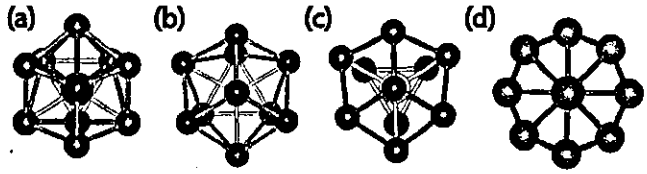

Figure 1. Representative lowest energy isomers of $X_{10}M$ clusters: (a) capped pentagon-rhombus structure (nearly 3-fold) as for $Si_{10}Ni$, (b) tetracapped trigonal prism as for $Pb_{10}Pt$, (c) a 3-fold symmetric structure as for $Si_{10}Pt$, and (d) bicapped square antiprism as for $Ge_{10}Ni$ and $Pb_{10}Pt$.

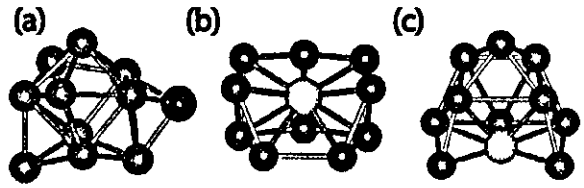

Figure 2. (a) Outside capping by the M atom as in $Si_{10}Pd$. Structures (b) and (c) show open structures for $Si_{10}Pt$ and $Ge_{10}Pt$, respectively.

one side of the Ni atom and a rhombus on the opposite side, as shown in Figure 1a. This is similar to the case of $Ge_{10}Co$ as well as to $Si_{10}Fe$ studied by Khanna et al.[13] However the HOMO−LUMO gap in $Si_{10}Ni$ is much larger with the value of 1.94 eV as compared to about 1 eV for $Si_{10}Fe$ showing that Ni doping is the most appropriate for the 10 atom Si magic clusters in agreement with the finding of large abundances of Co-doped anion clusters. This isomer is close to having 3-fold symmetry as it can be seen from the figure. An isomer with 3-fold symmetry is nearly degenerate and has the TTP structure with one triangular face opened up and Ni atom inside as shown in Figure 1b. The HOMO−LUMO gap is 1.98 eV. Since the GGA underestimates the gaps, the actual values are expected to be higher and to lie in the visible range. The magnetic moment of Ni atom gets completely quenched. An isomer with nearly 4-fold symmetry lies 0.77 eV higher in energy and acquires 2 μ_B magnetic moment in fully symmetric structure. The decahedral and pentagonal antiprism structures are found to have 2 μ_B magnetic moments in both the cases. Mpourmpakis et al.[13] also obtained a similar decahedral isomer for $Si_{10}Ni$. But it lies 0.67 eV higher in energy and has a small HOMO−LUMO gap of 0.33 eV. A decahedral structure was also obtained[13] for $Si_{10}Fe$. When a decahedral structure is optimized without spin-polarization, it transforms to a TTP structure with (surprisingly) slightly different bond lengths (Figure 1c) and it lies 0.27 eV higher in energy as compared to the lowest energy isomer. The HOMO−LUMO gap is also significantly different (1.49 eV). This structure has combined features of the pentagons and a capped hexagon as found in the fullerene-like and Frank−Kasper isomers[1] of the $Zr@Si_{16}$ cluster, respectively. A bicapped cube also changes to this isomer, whereas a bicapped square antiprism converts to the lower energy 3-fold structure (Figure 1b).

We also studied Ni outside Si_{10} on a triangular face of TTP. The converged structure (Figure 2a) lies 1.11 eV higher in energy. Therefore, Ni is favored inside the cage. The energy gain in doping Ni atom to Si_{10} is 5.13 eV, as